Chapter 7

Protective Coatings Based on PMMA–Silica Nanocomposites Reinforced with Carbon Nanotubes

Samarah V. Harb, Fábio C. dos Santos,
Sandra H. Pulcinelli, Celso V. Santilli,
Kevin M. Knowles and Peter Hammer

Additional information is available at the end of the chapter

http://dx.doi.org/10.5772/62808

Abstract

Polymethylmethacrylate–silica hybrids have been prepared using the sol–gel route by the radical polymerization of methyl methacrylate(MMA) using benzoyl peroxide (BPO) as a thermal initiator and 3-(trimethoxysilyl)propyl methacrylate(MPTS) as a coupling agent, followed by acid-catalyzed hydrolytic condensation of tetraethoxysilane (TEOS). Carbon nanotubes (CNTs) were first dispersed either by surfactant addition or by functionalization with carboxyl groups and then added at a carbon (CNT) to silicon (TEOS and MPTS) molar ratio (C_{CNT}/Si_{Hybrid}) of 0.05% to two different hybrid matrices prepared at BPO/MMA molar ratios of 0.01 and 0.05. Films of 2–7 μm thickness deposited onto carbon steel by dip-coating were characterized in terms of their microstructure and their mechanical, thermal and anticorrosive behavior. Atomic force microscopy and optical microscopy confirmed that there was a homogeneous dispersion of CNTs in the nanocomposites and that the surfaces of the films were very smooth. X-ray photoelectron spectroscopy (XPS) confirmed the nominal composition of the films while nuclear magnetic resonance showed that the connectivity of the silica network was unaffected by CNT loading. Thermogravimetric analysis and mechanical measurements confirmed an increase of thermal stability, hardness, adhesion and scratch resistance of CNT-loaded coatings relative to those without CNTs. Electrochemical impedance spectroscopy measurements in 3.5% NaCl solution interpreted in terms of equivalent circuits showed that the reinforced hybrid coatings, prepared at the higher BPO/MMA molar ratio used in this work, act as a very efficient anticorrosive barrier, with an impedance modulus up to 10^9 Ω cm^2.

Keywords: organic–inorganic hybrids, carbon nanotubes, mechanical reinforcement, structural properties, anticorrosive coating

1. Introduction

Organic–inorganic hybrids are a class of nanocomposite materials, which combine different components on the molecular or nanometric scale, resulting in hybrid systems that not only reflect the sum of the properties of the individual components but also are new materials with unique features. The blend of organic and inorganic phases interacting on the molecular scale combines properties such as processability, flexibility and hydrophobicity of the polymeric organic phases with thermal, chemical and mechanical stability of inorganic ceramic compounds. The nature, size and compatibility of the organic and inorganic phases are of critical importance, because they determine the transparency, homogeneity and stability of the hybrid material. The nature of the bonding at the interface between the phases is of particular significance for this class of nanocomposites. This can be used to classify these hybrid materials: the presence of relatively weak bonding such as van der Waals, dipole–dipole, hydrogen or ionic bonding is characteristic of a class I hybrid material, while strong covalent or ionic–covalent chemical bonding are both characteristic of class II hybrid materials [1].

The sol–gel process is possibly the most suitable method for the synthesis of hybrid materials because of the relatively mild synthesis conditions, the environmental compatibility, and, in particular, the possibility of combining a large number of precursors in different proportions. The simultaneous hydrolytic condensation of the inorganic precursor and polymerization of the organic species produces homogeneous nanocomposites with tunable properties. The multifunctionality of hybrid materials enables them to be used in a variety of applications such as drug delivery systems, optical and electrical devices, catalysts, photochromic devices and protective coatings [1, 2].

Among the large number of reported organic–inorganic nanocomposite systems, in which polymers such as epoxy, polyimide, acrylic and polyethylenimine phases are combined with inorganic oxides such as silica, alumina, zirconia, titania and ceria, one important hybrid class is the polymethylmethacrylate–silica (PMMA–silica) system. PMMA–silica nanocomposites have recently received considerable attention because of their ability to protect a wide variety of metal surfaces such as steels, stainless steels, aluminum alloys and magnesium alloys in an efficiently and environmentally compliant manner [3–5]. These alloys are particularly important for key industries such as the aerospace, automotive and offshore companies. However, most of these alloys suffer severe corrosion in maritime environments and even humid environments and therefore need appropriate surface passivation to survive for long periods in aggressive environments.

Corrosion is a spontaneous and irreversible reaction between a metal surface and its environment, resulting in significant economical losses, the failure of critical components and environmental problems. The prevention of corrosion, or at least its mitigation, is therefore one of the main challenges industrially worldwide. The application of protective coatings such as paints or resins, or those based on ceramic materials, is the most common way to improve the durability of metallic alloys significantly. However, organic coatings are relatively thick and can suffer poor thermal and mechanical stability and also a lack of adhesion, while coatings

http://dx.doi.org/10.5772/62808

based solely on ceramic materials are likely to be porous and suffer from intrinsic stress-induced cracking, leading to thickness limitations [3, 6].

Therefore, organic–inorganic hybrids have been developed to overcome the limitations of traditional coatings, forming an efficient and durable corrosion protection system for metallic surfaces. In the case of PMMA–silica hybrid nanocomposites, this corrosion protection is a consequence of the covalent bonding between PMMA and silica nodes through the coupling agent 3-(trimethoxysilyl)propyl methacrylate (MPTS), formed by three methoxy-silane groups linked by a nonhydrolysable Si–C bond to a methacrylate tail. This bonding mechanism produces a class II hybrid with a nanostructure of dense silica cross-link nodes bridged by short polymeric chains. As a consequence, the closely packed nanostructure acts as an efficient corrosion barrier against the uptake of aggressive agents [3, 4].

One drawback of most organic-inorganic hybrids is their relatively high polymer content of 60–80%; this leads to a reduced mechanical and thermal stability of these materials relative to ceramic systems. To overcome this limitation, carbon nanotubes (CNTs), known for their exceptional mechanical and thermal properties, are regarded as being the most suitable nanostructures to reinforce polymeric and hybrid materials. Thus, for example, in a recent study, Nafion® modified functionalized multiwall CNTs were dispersed in a PMMA–silica nanocomposite at carbon-to-silicon molar ratios of 0.1%, 1.0% and 5.0% [7]. The results of this study showed that the CNTs could be dispersed efficiently within the nanocomposite and that their presence did not affect the connectivity of the hybrid network. In addition, the coatings were able to maintain their high corrosion resistance, with an impedance modulus of about 10^7 Ω cm^2 in 3.5% NaCl solution [7]. However, no mechanical tests were performed in this study.

Other studies also report on hybrids and, in particular, on polymers modified by CNTs [8–10]. The development of nanocomposites with improved electrical conductivity, thermal stability and mechanical strength by incorporation of CNTs are the most cited objectives in these studies. For polyethylene–CNT composites containing CNTs in the range of 1–2.5 wt.%, an increase in electrical conductivity up to six orders of magnitude has been observed [8]. A uniform dispersion of CNTs in a polypropylene (PP) matrix has been shown to produce a substantial increase in thermal stability at extremely low loading levels of CNTs, attributed to the relatively large interfacial area common to the PP chains and the free radial scavenging CNTs [9]. For epoxy–CNT nanocomposites, in which the epoxy resin matrix was modified with 0.1 wt.% of amino-functionalized CNTs, an improvement in strain to fracture and an increase in Young's modulus from 3.29 GPa for the neat resin to 3.50 GPa for the nanocomposite have both been reported [10].

Protective hybrid coatings, modified with CNTs, have also been subject of a number of recent studies. Thus, for example, Fe_3O_4 nanoparticles attached to CNTs have been incorporated successfully at a concentration level of 3 wt.% into epoxy resin coatings deposited on carbon steel [11]. Experimental results showed a significant increase of coating adhesion and corrosion protection efficiency relative to coatings without both the Fe_3O_4 nanoparticles and the CNTs [11]. Epoxy–CNT composite coatings deposited on aluminum alloy 2024-T3 substrates at CNT levels of 0.1 wt% or 0.5 wt% showed a similar result with an improvement in adhesion strength,

wear resistance and rate of corrosion with CNT loading, the latter explained by a CNT-induced decrease of the level of open porosity within the coating [12]. Polypyrrole (PPy) coatings containing low levels of CNTs and chitosan deposited on St-12 steel have shown a significant improvement in corrosion protection relative to PPy coatings with an increase in the corrosion resistance in 3.5% NaCl solution from 176 Ω cm^2 for pure PPy to 861 Ω cm^2 for PPy–CNT–chitosan coatings [13]. This was attributed to the improved density and more compact structure of the PPy–CNT–chitosan composite relative to the pure PPy coatings [13]. A study of the corrosion protection performance of poly(N-methylpyrrole)-dodecylsulfate/CNT composite coatings on SAE 304 stainless steel was performed in 0.5 mol L^{-1} H_2SO_4 solution [14]. In these coatings, the CNTs were added as a second layer on top of the poly(N-methylpyrrole)-dodecylsulfate base layer, either by electrodeposition or by dispersing the CNTs in a Nafion® solution. The results also confirmed a significantly improved corrosion protection of the base layer coated with the Nafion®-dispersed CNTs. This was attributed by these authors to the electrostatic repulsion of corrosive anionic species by the negatively charged CNTs and Nafion® containing surface layers [14]. Using a similar strategy, a conductive coating based on PPy has been modified with 0.25–1 at.% of functionalized and nonfunctionalized CNTs and coated on 60/40 α/β brass [15]. The observed improvement of corrosion protection efficiency of the brass in 3.5% NaCl solution relative to coatings without CNTs was explained by the authors in terms of an increase in electrical conductivity of the CNT-loaded coatings to help form anodically protecting passive oxide films on the metal and also to the increase in tortuosity of the paths corrosive ions have taken through the coating to reach the passive film in order to attack it chemically [15]. The ability for deliberately undercured coatings with 20 wt.% of CNTs and microcapsules containing electrically conductive epoxy resin with self-healing property has also been demonstrated [16]. In this work, Bailey et al. used a novel electrotensile test. Upon cracking of the undercured coating during tensile testing, microcapsules in the crack path release the healing solvent ethyl phenyl acetate (EPA), enabling the subsequent reaction with residual hardener in the vicinity of the crack to make the matrix swell locally and cause cracks to be closed [16].

It is important to note that most as-synthesized CNTs consist of large aggregates or bundles insoluble both in water and in common organic solvents because of their enhanced polarizability induced by their cylindrical shape and hence the strong van der Waals' interactions between individual nanotubes [17]. Efficient dispersion of CNTs in a polymer matrix requires the initial disentanglement of these large aggregates and chemical compatibility between the CNTs and the polymer matrix to maintain a homogeneous and stable composite structure. This chemical compatibility can be induced either by preselecting a matrix which interacts electrostatically with CNTs or by modifying the interaction potential between the CNTs and the polymer by functionalization. A suitable functionalization of CNTs is able to increase their electrostatic potential, thereby reducing their tendency to agglomerate [9]. However, it is evident that if harsh treatment conditions are used, such as prolonged sonication or excessive chemical treatment, a high level of damage to the hexagonal nanotube structure can occur, leading to a significant loss of mechanical and electrical performance of the CNTs.

http://dx.doi.org/10.5772/62808

Alternative approaches have been developed to disperse individual CNTs by noncovalent functionalization employing a wrapping agent, typically a surfactant or an organic polymer. A successful separation of CNTs leading to a stable suspension in aqueous solutions of sodium dodecyl sulfate (SDS) surfactant with coaddition of saturated fatty acids was recently demonstrated [17]. Following on from previous work on PMMA–silica coatings containing CNTs [7], we have successfully prepared CNT-reinforced protective hybrid coatings on carbon steel in this study. The uniform dispersion of CNTs in the PMMA–silica matrix was accomplished using two different pretreatments: the functionalization by carboxylic groups and surfactant assistance using SDS for subsequent introduction in the PMMA–silica hybrids. Particular attention was paid to the extent to which CNTs could be incorporated successfully into the PMMA–silica matrix without compromising the excellent anticorrosive characteristics of the hybrids. The effects of the inclusion of CNTs on the morphological, structural, thermal, mechanical and electrochemical properties of the hybrid matrix were evaluated by optical and atomic force microscopy (AFM), nuclear magnetic resonance, X-ray photoelectron spectroscopy (XPS), mechanical testing and electrochemical impedance spectroscopy (EIS).

2. Experimental

2.1. Synthesis

All reagents were purchased from Sigma-Aldrich and used as received, apart from the methyl methacrylate monomer, which had been distilled before use to remove the ≤30 ppm amount of 4-methoxyphenol added as a polymerization inhibitor. The PMMA–silica hybrid synthesis consisted of radical polymerization of methyl methacrylate (MMA) and 3-(trimethoxysilyl)propyl methacrylate (MPTS) using the thermal initiator benzoyl peroxide (BPO) and tetrahydrofuran (THF) as a solvent, followed by hydrolysis and polycondensation of tetraethoxysilane (TEOS) and MPTS silane sites, catalyzed by nitric acid (pH 1). The following molar ratios were kept constant: MMA/MPTS = 8, TEOS/MPTS = 2, H_2O/Si = 3.5 and ethanol/H_2O = 0.5. The BPO/MMA molar ratio was fixed at a value of 0.01 and 0.05 to study the influence of CNTs in two different matrices designated BPO0.01 and BPO0.05.

The TEOS, MPTS and MMA molecular structures are shown in **Figure 1**. The siloxane bridges (C–Si–O) between the organic and the inorganic phase were derived from MPTS, a modified silicon alkoxide with a methacrylate group which acts as a coupling agent between the organic component, PMMA (polymerized MMA), and the inorganic component, silica. In the presence of acidified water, TEOS and MPTS form a silica network through sol–gel hydrolysis and condensation reactions, a process that converts a colloidal suspension (the sol) into a three-dimensional network (the gel). First, the alkoxy groups (O–CH_2–CH_3 and O–CH_3) are hydrolysed, forming silanol groups (Si–OH) and eliminating alcohol molecules (HO–CH_2CH_3 and HO–CH_3), and then silanol groups can react with one another or the initial reagent to yield Si–O–Si bonds [18].

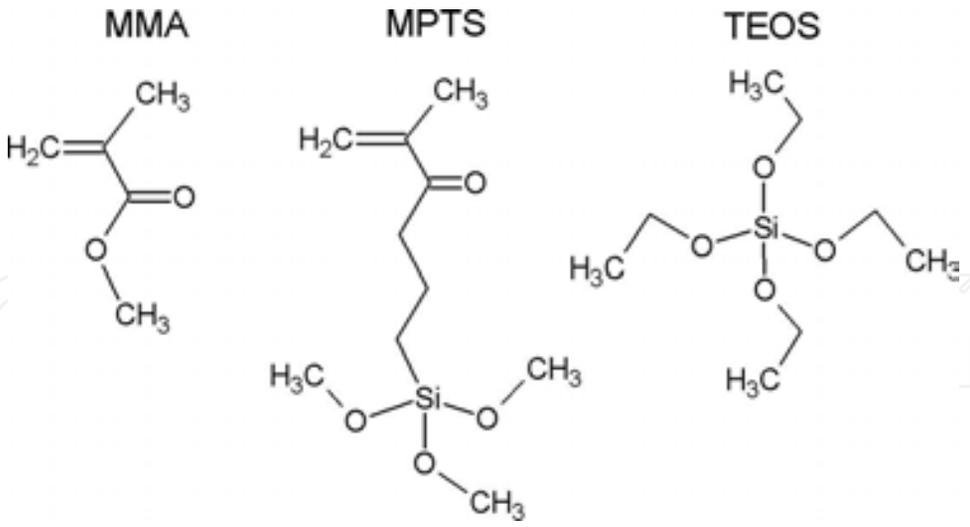

Figure 1. Molecular structures of the synthesis reagents.

Single-wall CNTs were purchased from Dropsens for incorporation into the two hybrids BPO0.01 and BPO0.05. In one pretreatment prior to their incorporation, the CNTs were dispersed using the method described by Alves da Cunha et al. [17], in which aqueous solutions of SDS surfactant (Sigma-Aldrich) and hexadecanoic acid (palmitic acid, Sigma-Aldrich) are used. The dispersion procedure, schematized in **Figure 2a**, starts from raw CNTs and is based on the nonpolar groups of SDS and palmitic acid promoting physical interaction with CNTs, while polar groups of these two chemicals interact with water [17]. After dispersion in SDS and palmitic acid, the CNTs were added at the end of the PMMA–silica hybrid synthesis, at a C_{CNT}/Si_{Hybrid} molar ratio of 0.05%, to the two matrices BPO0.01 and BPO0.05. The two nanocomposites produced in this manner were designated BPO0.01_CNT_SDS and BPO0.05_CNT_SDS, respectively.

In addition to the SDS method, dispersion through functionalization with carboxyl groups was also studied. In the second method, 0.1 g of CNTs was first put in a flask containing 75 ml of concentrated sulfuric acid (H_2SO_4, Sigma-Aldrich) and 25 ml of concentrated nitric acid (HNO_3, Sigma-Aldrich). The CNT-containing solution was then heated and stirred under reflux at 70°C for 2 h followed by 30°C for 4 h. Then, the functionalized CNTs were filtered through an ANOPORE 0.02 μm pore size membrane and washed with distilled water until the pH was 6. After this, drying was carried out at 70°C for 4 h under vacuum and at 200°C for 4 h in air (**Figure 2b**). The oxidation procedure with nitric acid and sulfuric acid adds carboxyl groups at the walls of the CNTs and enhances their solubility in the PMMA–silica hybrid. These functionalized CNTs (CNTCOOH) were dispersed using Nafion® and incorporated into BPO0.05 matrix in the inorganic phase at a C_{CNT}/Si_{Hybrid} molar ratio of 0.05%. The nanocomposite produced in this manner was designated BPO0.05_CNTCOOH.

After synthesis, the five homogeneous and transparent hybrid sols were used to deposit films onto 2.5 cm x 2.5 cm x 0.4 cm A1020 carbon steel substrates by dip-coating (3 immersions, each of 1 min, at a withdrawal rate of 14 cm min^{-1}, with air-drying intervals of 10 min between dips), with the remainder of the solutions placed in Teflon holders to obtain unsupported films, and

http://dx.doi.org/10.5772/62808

then heat-treated initially at 60°C for 24 h, followed by 160°C for 3 h. Prior to being dipped, the carbon steel substrates had all been sanded with 100, 300, 600 and 1500 grit sandpaper, washed with isopropanol for 10 min in an ultrasound bath and dried under nitrogen.

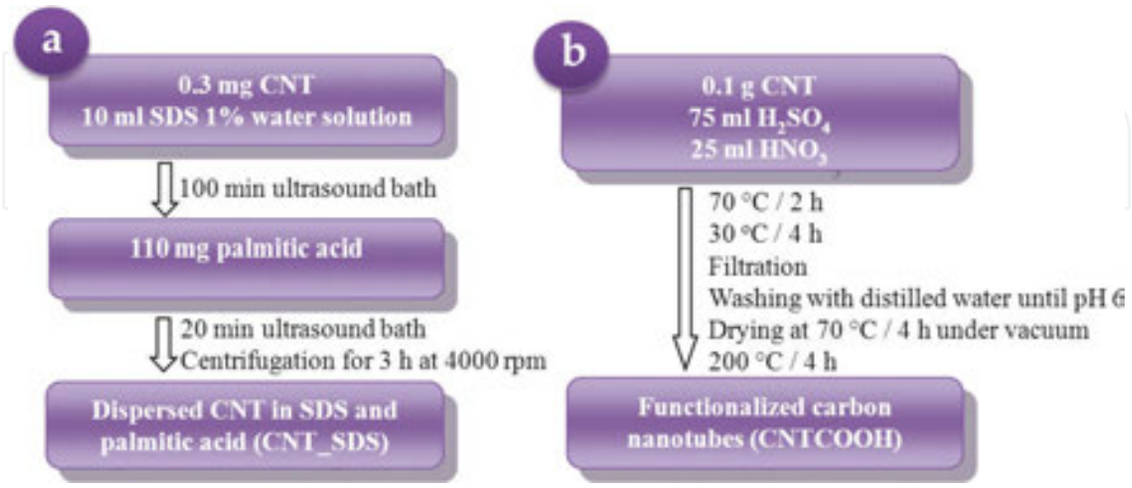

Figure 2. Experimental procedure for the dispersion of carbon nanotubes by (a) interaction with SDS and palmitic acid and (b) functionalization with carboxyl groups.

2.2. Characterization techniques

A JEOL 71500F field-emission gun scanning electron microscope (FEG-SEM) was used to acquire micrographs of raw and dispersed CNTs.

XPS was used for characterization of the CNTs and the hybrids by extracting the elemental compositions and monitoring the local bonding structure of carbon (C 1s), oxygen (O 1s) and silicon (Si 2p) Measurements were performed in a UNI-SPECS UHV surface analysis system, using Mg Kα radiation ($h\nu$ = 1253.6 eV) and a pass energy of 10 eV for high-resolution spectra. The inelastic background of the C 1s, O 1s and Si 2p photoemission peaks was subtracted using the Shirley baseline. The displacement due to charge accumulation was corrected by fixing the C–H component of the C 1s spectrum at 285.0 eV. The surface composition was determined from peak intensities corrected by the orbital sensitivity factors of the corresponding elements. The CasaXPS processing software was used for deconvolution of the spectra using combinations of Gaussian and Lorentzian functions (Voigt profiles) for analysis of the chemical bonding structure.

^{29}Si nuclear magnetic resonance spectroscopy (^{29}Si-NMR) measurements in the solid state were performed in a Varian Inova spectrometer operating at 300 MHz and 7.05 T, using a Larmor frequency of 59.59 Hz and tetramethyl silane (TMS) as an external standard. The spectra were obtained from Fourier transforms following a single excitation pulse of $\pi/2$ with a relaxation time of 2 s. The CasaXPS processing software was used for deconvolution of the spectra using Voigt profiles.

The thickness of each coating was determined using a Filmetrics F3-CS optical interference system. AFM was used to evaluate the surface morphology of the coatings and to determine their roughness. Agilent Technologies Model 5500 and NX10 Park System atomic force microscopes were used in tapping mode with a silicon cantilever. The results were analyzed using Gwyddion software. RMS (root mean square) roughness values were obtained from 1 μm × 1 μm topography images of the hybrid coatings deposited on the A1020 carbon steel.

Thermogravimetric analysis (TGA) of the five unloaded and CNT-loaded hybrids, each in the form of unsupported films, were carried out in a TA Instruments STD Q600 analyzer. The samples were heated at a rate of 5°C min^{-1} from 25°C to 800°C, under 100 mL min^{-1} of nitrogen flow.

Nanoindentation measurements were carried out in a Nano Indenter® XP system, MTS, equipped with TestWorks 4 Professional level software. A diamond tip with Berkovich geometry was used. For each sample, nine measurements were performed, with 100 μm spacing between each indentation. The input parameters were Poisson ratio (0.35), depth limit (140 nm), allowable drift rate (0.8 nm/s), frequency target (45 Hz) and percent unload in stiffness calculation (50%). Use of the continuous stiffness measurement (CSM) method allowed the continuous determination of the contact stiffness during loading, providing more accurate results. This was achieved by superimposing a small oscillation on the primary loading signal and by analyzing the resulting response of the system using a lock-in amplifier. The hardness and elastic modulus were obtained as a continuous function of depth from a comparison of samples indented in the range of 60–120 nm. To avoid effects on the nanomechanical properties of the films from the underlying steel substrates, the maximum penetration depth for the indentation experiments was set at less than 10% of the coating thickness [19].

Microscratch measurements were performed using homemade equipment at the National Physical Laboratory (Teddington, London, U.K.) to evaluate the scratch resistance and the adherence of the coatings to the A1020 carbon steel substrates. For each sample, 3 parallel tracks of 6 mm length with 1 mm spacing between the tracks were made using a linearly increasing load (from 2 mN to 100 mN), with a diamond tip with spherical conical geometry and 10 μm radius. For CNT-loaded hybrids, further microscratch experiments were undertaken where the load was increased up to a maximum of 240 mN. The measurements also provided the coefficient of friction as a function of the track distance. The tracks were analyzed using a Nikon Measuring Microscope MM-60, coupled with a Nikon SC-213 Digital Counter, which enabled the critical load at which delamination started to be determined.

The anticorrosion efficiency of the hybrid coatings deposited on the A1020 carbon steel was analyzed by EIS using a Gamry Potentiostat Reference 600. The impedance data were collected once a week, until failure, over a frequency range from 10^{-2} Hz to 10^{4} Hz with 10 points per decade and signal amplitude of 10 mV (rms) in an electrochemical cell containing 80 ml of 3.5% NaCl solution at 25°C. The electrochemical cell consisted of a $Ag|AgCl|KCl_{sat}$ reference electrode, a platinum mesh counter electrode, a platinum electrode connected to the reference electrode through a 0.1 μF capacitor and the working electrode of either coated or uncoated carbon steel. The experimental data were fitted with equivalent electrical circuits using Zview software to analyze the EIS response.

http://dx.doi.org/10.5772/62808

3. Results and discussion

3.1. CNT characterization

Van der Waals' forces between CNTs cause their agglomeration in the form of dense bundles. Commercial CNT powder consists of dense particles (**Figure 3a**), which comprises the bundles of CNTs (**Figure 3b**). It is evident from **Figure 3c** and **Figure 3d** that both procedures used for dispersing the CNTs were successful.

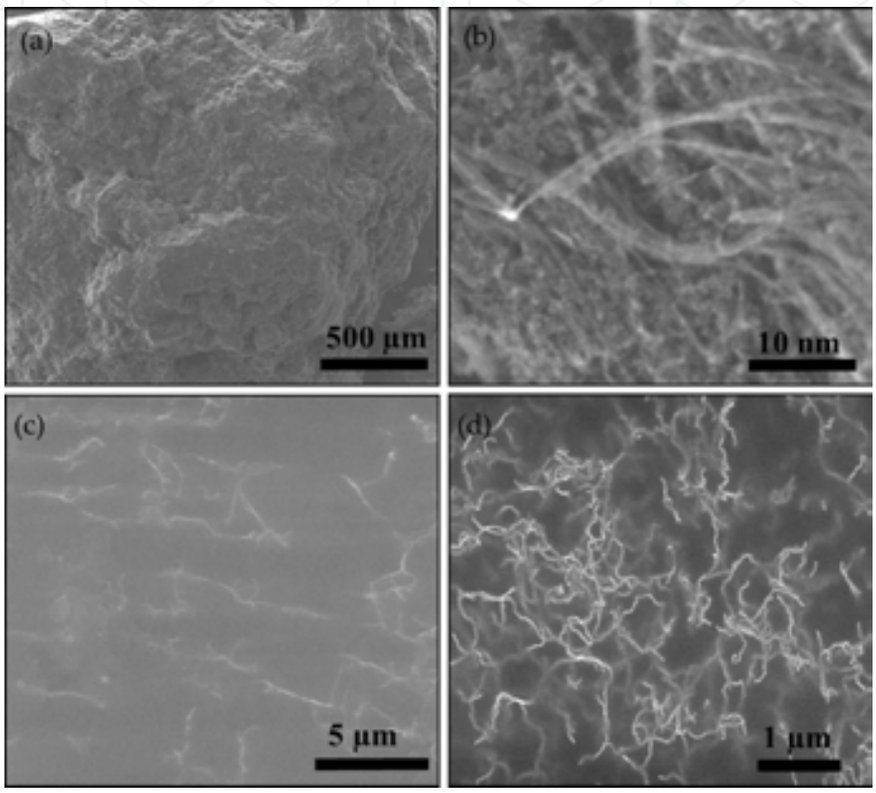

Figure 3. FEG-SEM micrographs of carbon nanotubes (a, b) commercial powder, (c) dispersed in SDS and palmitic acid and (d) functionalized and dispersed in the precursor solution.

CNTs have a peculiar XPS C 1s spectrum with the presence of a predominant aromatic C-C-sp^2 component and characteristic π plasmon transitions, the intensities of which scale with the degree of order of the hexagonal carbon structure. XPS C 1s spectra of pure and functionalized CNTs are presented in **Figure 4**. Quantitative XPS analysis can detect all elements except hydrogen and helium. Discounting the presence of hydrogen, the raw CNTs are composed of 93.2 at.% of carbon and 6.8 at.% of oxygen (**Figure 4a**), partially related to surface contamination by oxygenated hydrocarbon groups of adventitious carbon. The following characteristics indicate a highly aromatic structure: the presence of plasmon peaks (collective $\pi \rightarrow \pi^*$ transitions at ~291 eV and ~394 eV) and the narrow and intense component related to aromatic C-C-sp^2bonds (284.4 eV) with FWHM (full width at half maximum) of about 0.9 eV and a peak area of 65.5% [20]. The high energy components related to C–O, C=O and O–C=O bonds, which

can also be observed in the O 1s XPS spectrum (**Figure 4b**), show the presence of ether/alcohol, carbonyl and carboxyl groups on the surface of the nanotubes, associated mainly with the presence of adventitious carbon responsible for the C–H component at ~285 eV. After functionalization, the O–C=O component increases significantly (**Figure 4c** and **4d**) due to the linking of these groups to the walls of the nanotubes, aiding the dispersion of CNTs in the hybrid matrix through their polarity. The degree of functionalization of nanotube walls defined as the intensity ratio I(O–C=O)/I(C-C-sp^2) was 0.3.

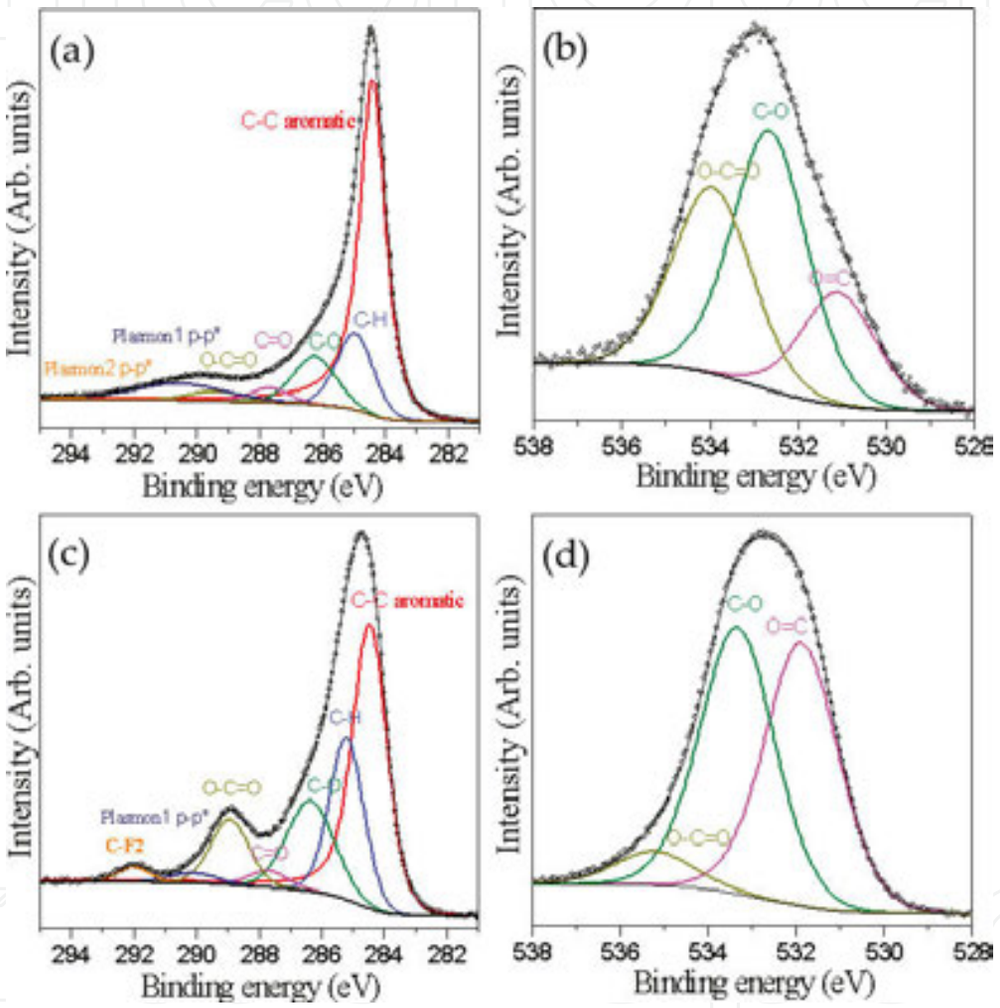

Figure 4. (a) C 1s and (b) O 1s XPS spectra of the as-received CNTs and (c) C 1s and (d) O 1s XPS spectra of functionalized CNTs.

3.2. PMMA–silica hybrid characterization

3.2.1. Surface morphology

All the PMMA–silica hybrid coatings deposited on the A1020 carbon steel were transparent with a homogeneous, colorless appearance. A representative image of one of the 2.5 cm x 2.5

http://dx.doi.org/10.5772/62808

cm x 0.4 cm coated samples is shown in **Figure 5a**. Inspection by optical microscopy performed on free standing hybrids in transmission mode confirmed the uniformity of these coatings (e.g., **Figure 5b**) and indicate a very good dispersion of CNTs in the nanocomposites.

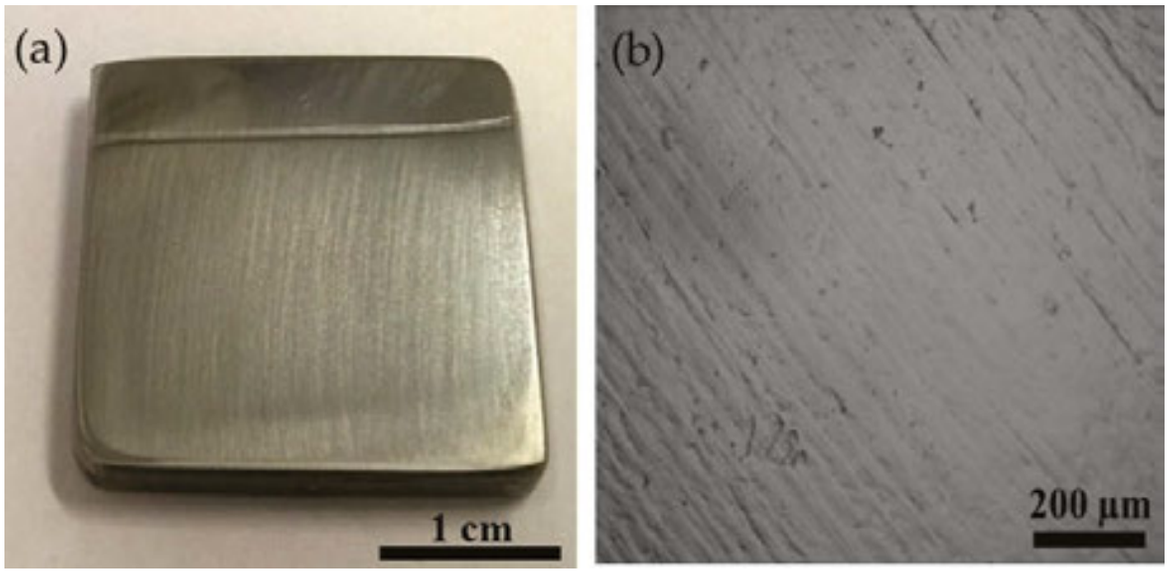

Figure 5. (a) Representative image of BPO0.01_CNT_SDS coating deposited on A1020 carbon steel and (b) optical microscopy image showing a detail of the BPO0.01_CNT_SDS transparent film. Parallel lines in (b) are related to the steel substrate morphology.

One effect caused by increasing the BPO/MMA molar ratio from 0.01 to 0.05 was the reduced gel time of the hybrid sol. This occurred because of the enhanced polymerization rate induced by the increase in the number of radicals of the BPO thermal initiator, leading to a higher viscosity of the solution. In addition to this effect, the inclusion of CNTs also increased the viscosity of the solution prior to dip coating. Together, these two effects account for the trend in the observed hybrid coating thicknesses shown in **Table 1**.

Sample name	BPO/MMA molar ratio	Thickness (µm)	Surface RMS roughness (nm)
BPO0.01	0.01	2.8	0.4
BPO0.01_CNT_SDS	0.01	5.7	0.4
BPO0.05	0.05	3.5	0.4
BPO0.05_CNT_SDS	0.05	6.6	0.5
BPO0.05_CNTCOOH	0.05	4.9	0.2

Table 1. Thickness and surface roughness of pure and CNT-containing PMMA–silica hybrids prepared at different BPO/MMA molar ratios.

AFM topography images obtained for pure PMMA–silica films and for those containing well-dispersed CNTs showed that each of the five hybrids presented a very smooth and uniform

surface morphology (**Figure 6**). No defects, pores, cracks or inhomogeneities were observed on the coated samples. The RMS roughness (R_{RMS}) extracted from AFM measurements (Table 1) showed very low values of <0.5 nm for all coatings, confirming the homogeneity of the films and the efficient dispersion of CNTs within the hybrid matrices. The BPO0.01_CNT_SDS surface morphology is shown in the high-resolution AFM image in **Figure 7**. The local smoothness of the surface is confirmed in this image, while there is also indication for a possible presence of a single CNT on the surface.

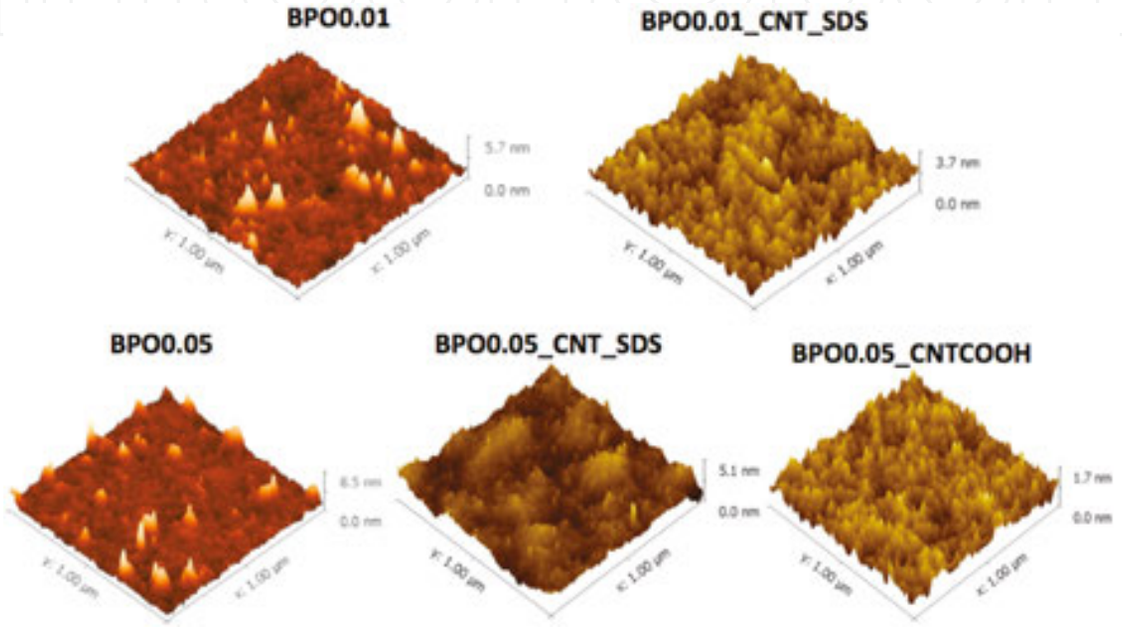

Figure 6. AFM images of all hybrid coatings deposited on carbon steel.

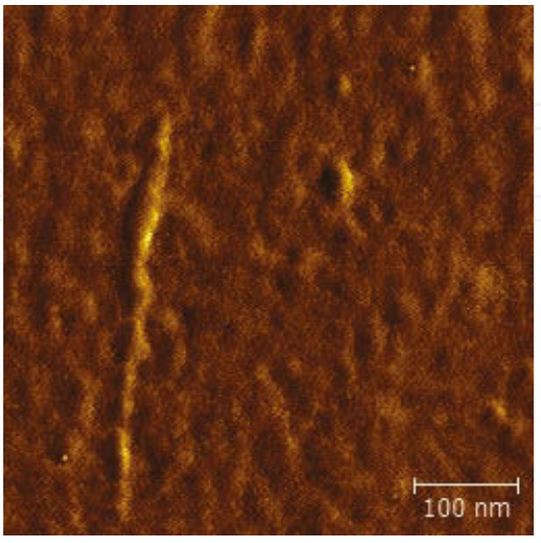

Figure 7. High-resolution AFM image of the BPO0.01_CNT_SDS sample.

http://dx.doi.org/10.5772/62808

3.2.2. Bonding structure

XPS analysis showed that the composition of all hybrids was very similar, with values close to the nominal atomic percentages of 62 at.% of carbon, 32 at.% of oxygen and 6 at.% of silicon, with an experimental error of ±5%. Representative spectra of carbon, oxygen and silicon, deconvoluted into their structural components, are presented in **Figure 8**. The C 1s spectrum, shown in **Figure 8a**, has four components related to C–H, C–C–O, C–O and O–C=O bonds present in the PMMA and MPTS molecules (**Figure 8d**) [21]. The carbon underlined corresponds to the atom that was analyzed. The O 1s spectrum (**Figure 8b**) was fitted with three components, associated with O–C=O and O=C bonds of PMMA and MPTS, and O–Si bonds of the inorganic network, observed also in the Si 2p spectrum (**Figure 8c**). For completely condensed SiO_2 phase the well-known binding energy of the Si 2p peak is located at 103.5±0.2 eV [21]. As the condensation reaction was incomplete, it is possible that the observed binding energy shift to a lower value of 103.1 eV is caused by some remaining silanol groups (Si–OH) from TEOS and MPTS hydrolysis and condensation. The addition of CNTs to the PMMA–silica hybrids had no effect on the XPS spectra because the additional carbon concentration level of 500 ppm from the nanotubes was below the 3000 ppm detection limit of carbon.

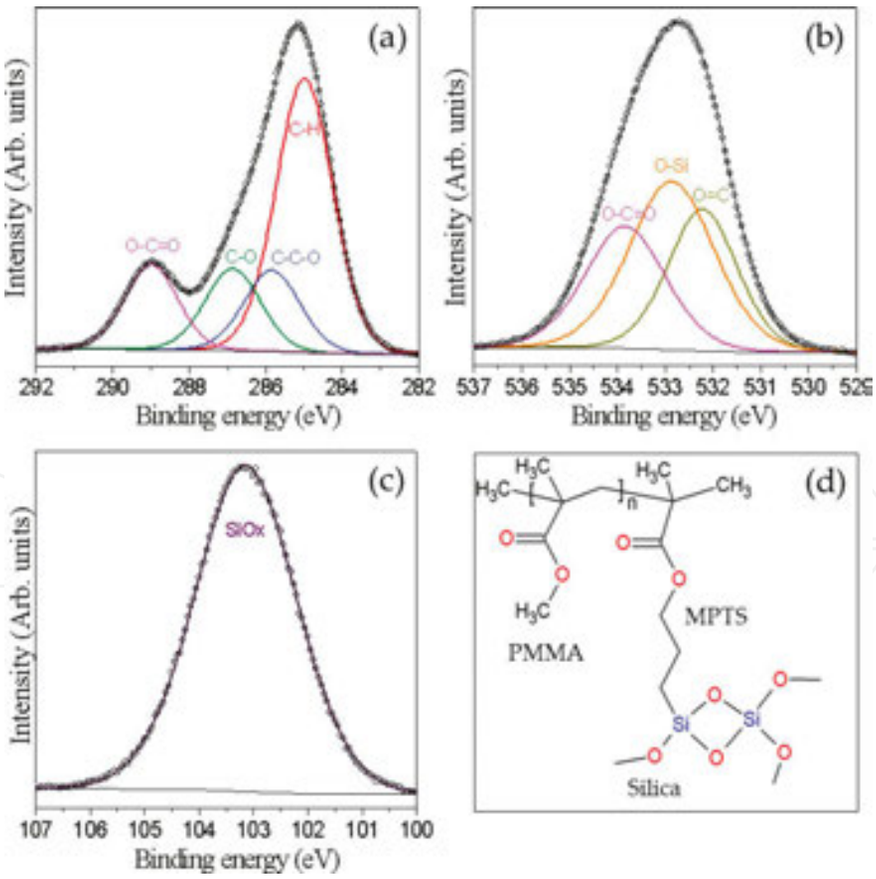

Figure 8. Representative (a) C 1s, (b) O1s and (c) Si 2p XPS spectra of a PMMA–silica hybrid and (d) a schematic of the PMMA–silica hybrid structure.

^{29}Si-NMR analysis also allows the identification of the local chemical bonding structure and the quantitative evaluation of the connectivity of the inorganic phase. To determine the influence of the CNTs on the inorganic silica network, NMR was used to compare the pure and CNT-containing hybrids. Representative spectra are shown in **Figure 9** for a CNT-containing sample and a pure sample. Both spectra have two groups of peaks corresponding to T^i (i = 1, 2, 3) and Q^j (j = 2,3,4) structures shown in **Figure 10**. These two forms of local structures arise as a consequence of the MPTS and TEOS precursor species, respectively. The peaks at chemical shifts of −45, −55 and −63 ppm correspond to T^1, T^2 and T^3 environments, respectively, while the peaks at chemical shifts at −90, −100 and-110 ppm are associated with Q^2, Q^3 and Q^4 environments, respectively (**Figure 10**) [22]. The connectivity of the inorganic phase, defined as degree of polycondensation (C_d), was determined from the fitted Voigt profiles using the following equation:

$$C_d = \left(\frac{T^1 + 2T^2 + 3T^3}{3} + \frac{Q^1 + 2Q^2 + 3Q^3 + 4Q^4}{4} \right) \times 100 \quad (1)$$

The degree of polycondensation determined for BPO0.01 was 78±1%, meaning that about 80% of the silicon atoms are bonded to other silicon atoms through Si–O–Si oxygen bridges. Similar C_d values were obtained for the CNT-containing hybrid BPO0.01_CNT_SDS, indicating that CNT loading did not affect the connectivity of the silica phase.

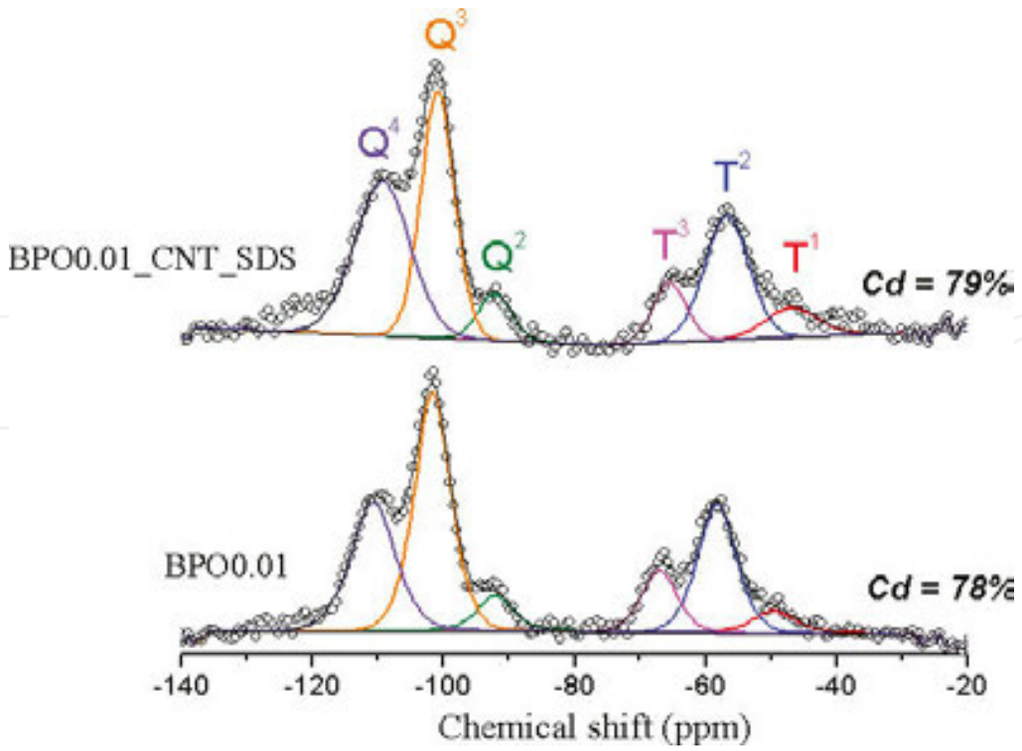

Figure 9. ^{29}Si-NMR spectrum from the BPO0.01 and BPO0.01_CNT_SDS samples.

http://dx.doi.org/10.5772/62808

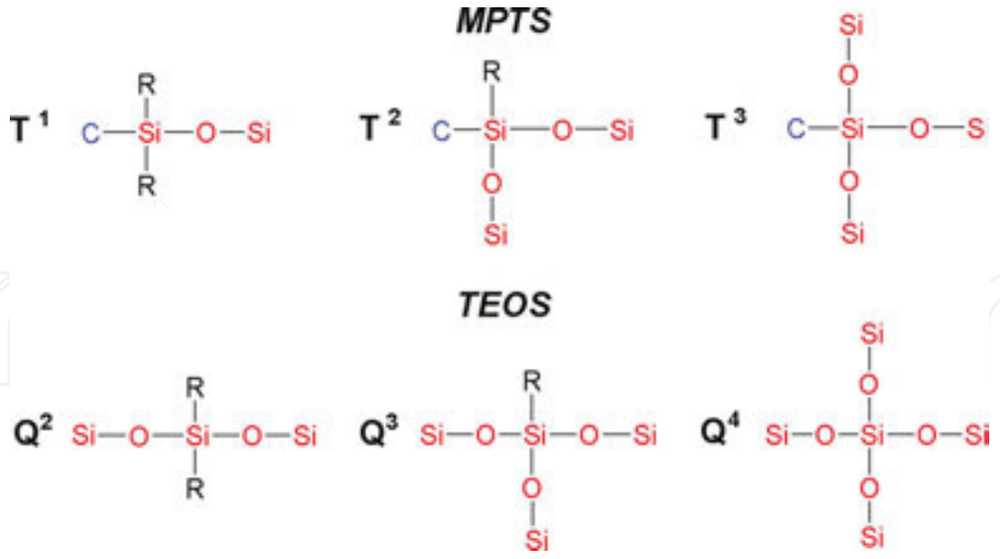

Figure 10. Schematic representation of T^i and Q^j structures. 'R' indicates OH or OCH_3 groups in MPTS or OCH_2CH_3 in TEOS.

3.2.3. Thermal properties

Thermogravimetry examines the overall connectivity of the hybrid network in terms of the thermal stability of the hybrid materials in different atmospheres. Under nitrogen, PMMA degrades in 3 events as the temperature increases: scission of head-to-head linkages at about 200°C (T_1), scission of vinylidene chain-ends at about 300°C (T_2) and finally random scissions of the polymer chains due to the rupture of head–tail segments at about 400°C (T_3) [23, 24]. The T_4 event at higher temperatures around 500°C is due to the dehydration of the remaining silanol groups of the silica network, detected in the XPS Si 2p spectra of **Figure 8** [23]. Thermogravimetric (TG) curves and their derivatives (differential thermogravimetry curves – DTG curves) for all the hybrid samples are shown in **Figure 11**. The onset temperature, T_0, which is a measure of the thermal stability of each material, is defined as the temperature at which a 5 % weight loss occurs. The temperatures of all events and the percentages of the silica and graphitic residues at 800°C are listed for the five hybrid samples in **Table 2**.

Comparing the DTG results obtained for the BPO0.01 and BPO0.05 matrices (**Figure 11b**), it is apparent that the higher quantity of BPO leads to an increase in the degree of polymerization and thus to a higher thermal stability, so that the low-temperature events seen in BPO0.01 are suppressed in BPO0.05. It can be seen from the data in Table 2 that all five hybrids are stable up to 200°C, with sample BPO0.01_CNT_SDS having the highest thermal stability (220°C). Furthermore, considering that the T_4 peak related to the dehydration of silanol is almost constant and that all loaded samples have the same CNT concentration, the residue formed mainly of pure silica (SiO_2) and some remaining graphitic phase can be used to estimate the fraction of the organic phase. The observation that hybrids prepared at the lower BPO to MMA ratio of BPO0.01 have about 4% higher amount of residue than those synthesized at the higher

ratio of 0.05 is consistent with an increase in polymerization and a higher fraction of the polymeric phase in the BPO0.05-based samples.

It is also interesting to note that the addition of the CNTs to BPO0.01 enhanced its thermal stability. In addition to the 15°C increase in T_0, the first two depolymerization events (T_1 and T_2) shifted by about 50°C to higher temperatures (Table 2). The T_3 disintegration event increased by 20°C. This result is similar to that found by Jin et al. [25], in which T_3 was shifted upwards by 30°C for a PMMA matrix containing 26 wt.% of CNTs, a concentration significantly higher than reported in this work. The retardation effect was attributed by Jin et al. to interactions between the carbon nanostructure and macroradicals generated during the depolymerization, as suggested by Troitskii et al. [26]. In contrast, the BPO0.05 matrix shows values of the thermal degradation events almost unchanged by the presence of CNTs. Compared to the BPO0.01 matrix, this behavior can be understood in terms of a more stable structure of the BPO0.05 matrix induced by the higher degree of polymerization.

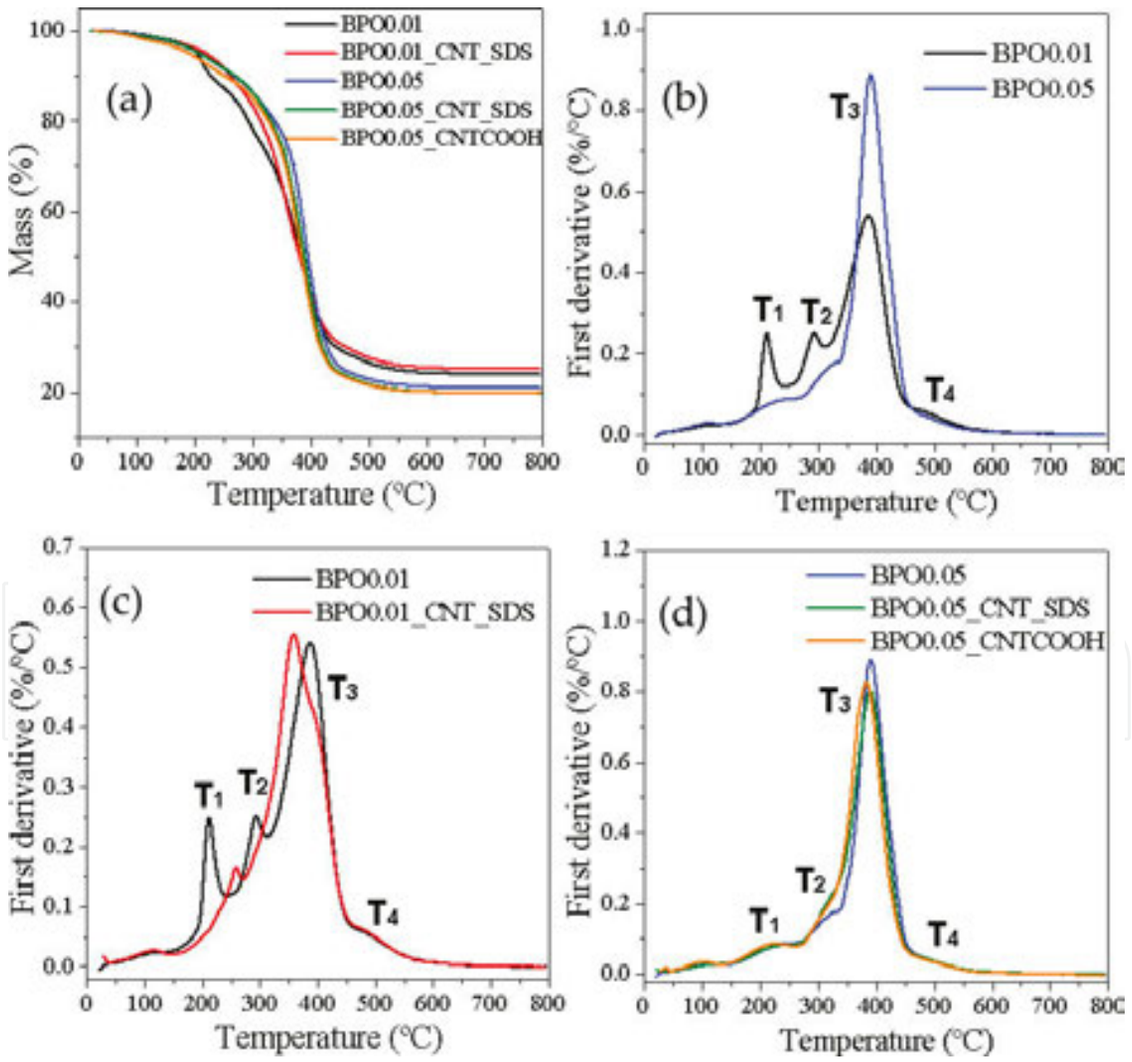

Figure 11. (a) TG curves and (b–d) DTG curves of the five hybrid samples.

http://dx.doi.org/10.5772/62808

Hybrid	T_0 (°C)	T_1 (°C)	T_2 (°C)	T_3 (°C)	Residue (%)
BPO0.01	205	210	290	385	24.0
BPO0.01_CNT_SDS	220	255	355	390	25.1
BPO0.05	208	220	310	390	21.1
BPO0.05_CNT_SDS	209	220	310	390	19.8
BPO0.05_CNTCOOH	192	220	310	385	20.1

T_0: Temperature of 5% weight loss, and temperatures T_1 of the first, T_2 of the second and T_3 of the third degradation event.

Table 2. The characteristic temperatures of the degradation events of PMMA–silica hybrid and the residue percentage obtained by thermal analysis in nitrogen atmosphere.

Our work and a number of other studies investigating the reinforcement effects by CNTs in diverse organic and hybrid matrices all come to the same conclusion: the modification improves the thermal stability of the composite. Thus, for example, in a recent study, Sabet et al. [27] used 5 wt.% of multiwall CNTs (MWCNTs) functionalized with carboxylic groups to reinforce an organic–inorganic hybrid matrix based on polyhedral oligomeric silsesquioxane (POSS). The approach involved a covalent conjugation between the CNTs and the POSS molecules through amide bonds. These authors observed that the decomposition under nitrogen of the neat POSS started at 265°C, and a complete weight loss was observed at 500°C. The POSS–MWCNT composite exhibited a fairly stable thermal behavior from room temperature to 200°C, and only 40% of weight loss by 1000°C measured by TGA.

Zhang et al. [28] coated functionalized MWCNTs with silica nanospheres, and subsequently introduced these into PMMA at a loading level of 4.28 wt.% to make it more flame resistant. TGA of the resultant PMMA/silica/MWCNT nanocomposites heated at 20°C min^{-1} indicated that the MWCNT/silica combination not only increased the temperature indicating 5% weight loss from 300°C of PMMA to 343°C, but also the temperature of the maximum rate of degradation increased from 338°C for PMMA to 387°C for the nanocomposites. These results, supported by cone calorimeter tests and scanning electron microscopy, showed that the MWCNT/silica combination introduced into the PMMA noticeably improved the thermal stability and flame retardancy of PMMA by in effect forming a surface thermal barrier layer during burning which helped to protect the underlying bulk from exposure to the external heat source.

Fraser et al. performed an in situ polymerization of PMMA in the presence of a low 0.1 wt.% concentration of either raw single-wall CNTs (SWCNTs) or acid-treated SWCNTs [29]. Although these transparent nanocomposites had slightly lower temperatures at which 10% weight loss had occurred in TGA when heated at 10°C min^{-1} in comparison with commercial PMMA, the temperature corresponding to the maximum rate of degradation increased by 8°C for the composites with the raw SWCNTs and by 18°C for the composites with acid-treated SWCNTs. Interestingly, these authors also showed using Raman spectroscopy that acid

treating of the SWCNTs enabled them to bind covalently with the PMMA, rather than merely be in contact with it, as was the case with the raw SWCNTs.

The thermal analysis results obtained by Xiong et al. for polyurethane (PU) covalently linked with 2 wt.% of amino-functionalized MWCNTs indicate that the temperature at which the maximum rate of degradation occurs increased from 408°C for PU to 419°C for the composite in TGA experiments with heating rates of 20°C min^{-1}, once again indicating an improvement of thermal stability of a polymer matrix with the addition of CNTs [30]. Another TGA study, this time with a heating rate of 10°C min^{-1} on PU nanocomposite coatings modified with 5 wt. % MWCNTs, showed that the temperature at which there was complete decomposition of the matrix PU increased by 21°C with the introduction of the MWCNTs [31]. This was explained by the authors in terms of the relatively inert MWCNTs retarding the free movement of the PU chains.

Overall, it can be concluded that the improvement of the thermal stability of CNT-modified polymers and hybrid nanocomposites, reported by a number of laboratories, can be attributed to a variety of factors, all of which are related to the intrinsic thermal stability of CNTs, the effects of radical scavenging and by forming a physical barrier making it difficult for volatile products in the matrix to escape from the bulk.

3.2.4. Mechanical properties

Nanoindentation curves provide continuous values of Young's modulus and hardness during loading as a function of displacement (e.g., **Figure 12**). The average Young's modulus and hardness values and the corresponding standard deviations and coefficients of variation for the five nanocomposites, determined from displacements between 60 and 120 nm, are summarized in **Table 3**.

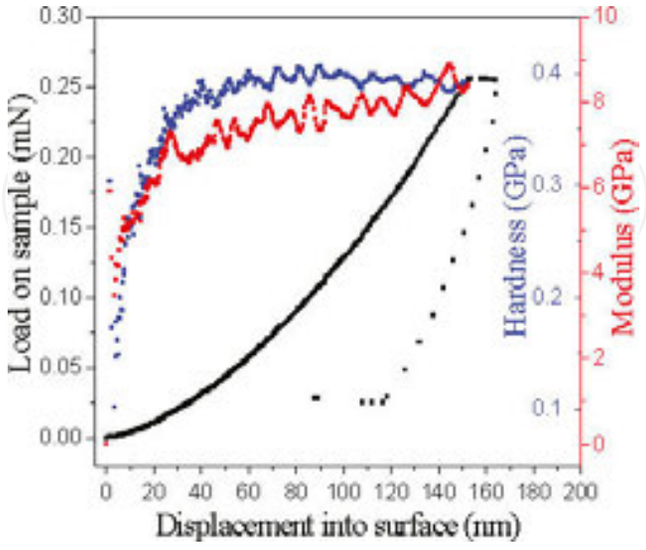

Figure 12. Representative loading and unloading nanoindentation curves for sample BPO0.01 from which hardness and Young´s modulus values were obtained.

http://dx.doi.org/10.5772/62808

Nanoindentation results show a coating hardness between 0.38 ± 0.4 GPa and 0.49 ± 0.6 GPa for all samples, values about twice as high as those for PMMA (0.22–0.26 GPa), but, not surprisingly, significantly lower than amorphous SiO_2 (7–9 GPa) [32]. Young's modulus values were in the range between 6.6 ± 0.3 GPa and 7.7 ± 0.1 GPa, about three times higher than pure PMMA (2.24–3.24 GPa), but about one order of magnitude lower than the elastic modulus of silicon oxide (73 GPa). These values represent a significant improvement of hardness and stiffness compared to pure acrylic, despite the presence of more than 70% polymethacrylate groups in the hybrid [33]. The inclusion of CNTs only produced a significant increase in hardness for the BPO0.05_CNT_SDS coating, with an increase of some 20% in comparison with the hardness of the BPO0.05 reference sample.

Sample	Young's modulus (GPa)			Hardness (GPa)		
	Mean	Std. dev.	% COV	Mean	Std. dev.	% COV
BPO0.01	7.849	0.398	5.07	0.400	0.042	10.41
BPO0.01_CNT_SDS	6.597	0.346	5.25	0.379	0.036	9.58
BPO0.05	7.749	0.137	1.77	0.413	0.012	2.83
BPO0.05_CNT_SDS	7.718	0.454	5.88	0.491	0.059	12.07
BPO0.05_CNTCOOH	7.501	0.154	2.06	0.431	0.014	3.23

Table 3. Young's modulus and hardness values, determined from indentations between 60 and 120 nm deep.

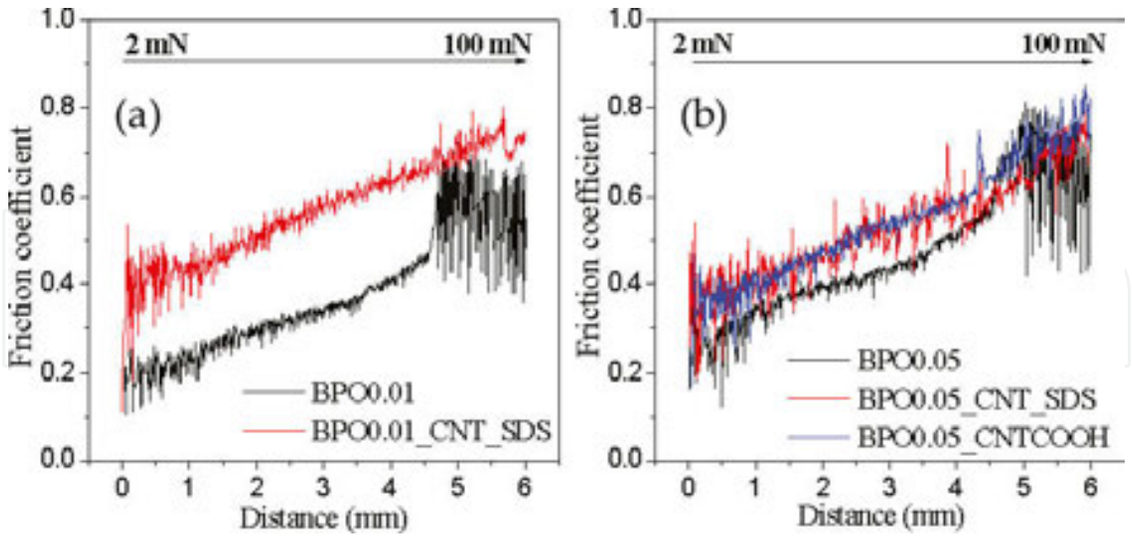

Figure 13. Microscratch curves (a) for BPO0.01 matrix coatings and (b) for BPO0.05 matrix coatings.

Scratch testing is a widely used, fast and effective method to provide information on the level of adhesion, resistance to scratching, the mechanism of fracture, the coefficient of friction

and the wear characteristics of coatings. In a typical experiment, a coating is scratched with increasing normal force using a diamond stylus. The track is then analyzed by optical or electron microscopy to determine the mechanism of mechanical failure, such as coating detachment (loss of adhesion to the substrate), cracking and plastic deformation. The scratch test provides the coefficient of friction, defined as the ratio of the applied load and the normal load, directly.

Curves of the coefficient of friction as a function of scratch distance (microscratch curves) for all hybrid coatings are shown in **Figure 13**. The increase of the friction coefficient is associated with an increase in scratch resistance (friction force), while the critical load for delamination is related to the difficulty in breaking the adhesive interaction between the coating and the metal substrates. The scratch tracks, shown in **Figure 14**, were analyzed by optical microscopy to determine the failure mechanism and the critical load for film cracking and delamination.

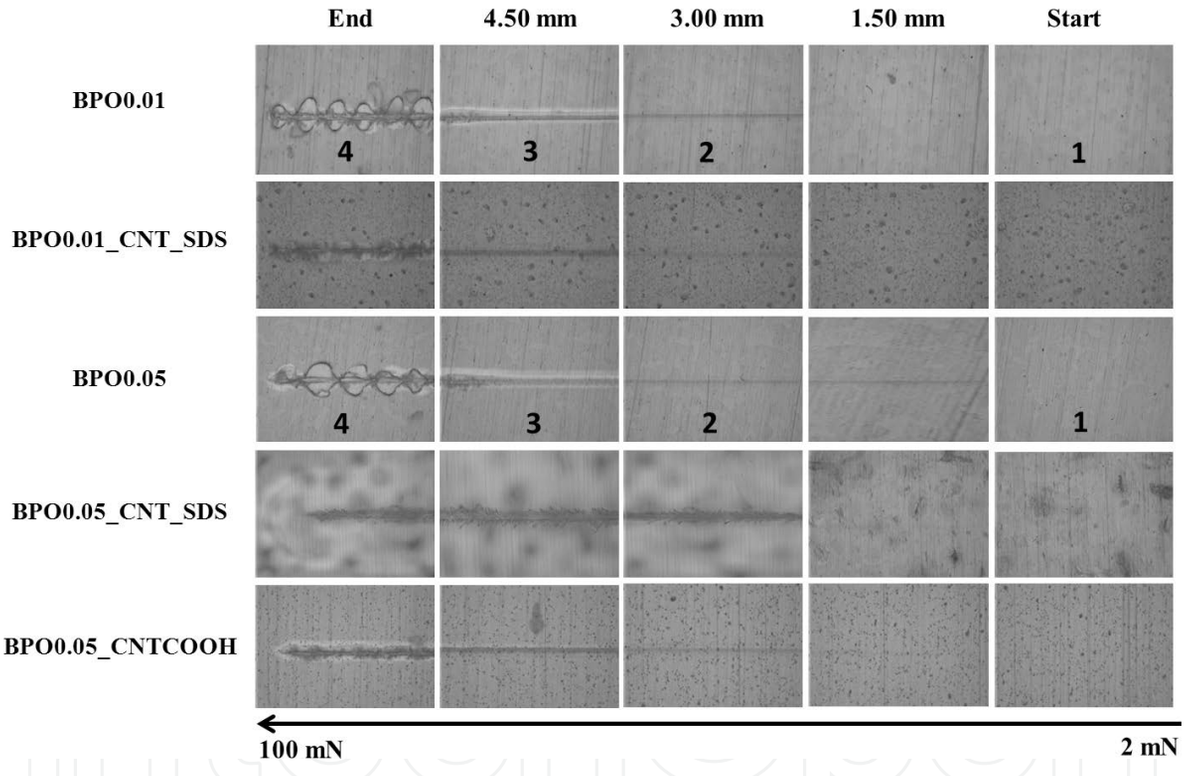

Figure 14. Optical microscopy of the five hybrid coatings deposited on A1020 carbon steel after scratch testing.

As is evident from **Figure 14**, the PMMA–silica reference samples (BPO0.01 and BPO0.05) were the softest coatings, showing four deformation stages with increasing force: (1) elastic deformation, (2) plastic deformation, (3) cracks and (4) delamination. The critical loads for delamination were 78 mN for BPO0.01 and 84 mN for BPO0.05, marked by the start of strong noise on the microscratch curves shown in **Figure 13**. The hybrids containing CNTs showed a higher scratch resistance and better adhesion to the A1020 steel substrate. Most interestingly, the BPO0.01_CNT_SDS coating showed an extreme reinforcement effect, with a higher

http://dx.doi.org/10.5772/62808

coefficient of friction than carbon steel (0.5) [34] and no delamination up to a load of 240 mN (**Figure 15a**), the maximum load capacity of the equipment. BPO0.05_CNT_SDS and BPO0.05_CNTCOOH had critical loads for delamination of 133 mN (**Figure 15b**) and 122 mN (**Figure 15c**), respectively, both are higher than those obtained for the BPO0.05 matrix. These results confirm that the intrinsic mechanical properties of CNTs, i.e., the high elastic modulus (~1.4 TPa) and the high strength (50–500 GPa), contribute to a significant reinforcement of the hybrid [35]. The strong adhesion of the hybrid film to the carbon steel is a consequence of the covalent interaction between the hydroxyl groups of the substrate and the silanol groups of the inorganic part of the hybrid. The increased mechanical strength of the hybrids, induced by the incorporation of CNTs, increases the critical force for delamination, thus extending the functionality of protective PMMA–silica coatings to conditions where abrasive forces act in an aggressive environment, such as in reactors for the acidic processing of sugar cane, for example.

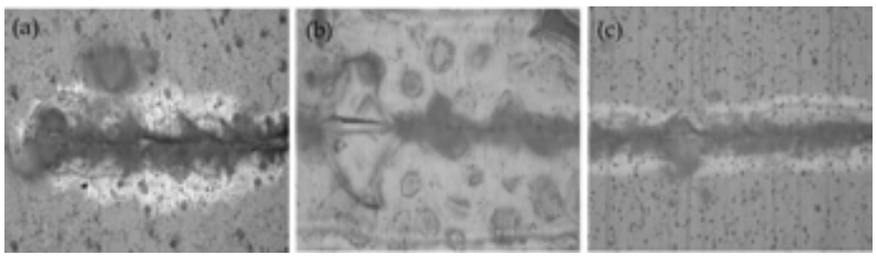

Figure 15. Optical microscopy of (a) the BPO0.01_CNT_SDS coating after scratch testing to a load of 240 mN, (b) the BPO0.05_CNT_SDS coating after scratch testing to a load of 133 mN and (c) the BPO0.05_CNTCOOH coating after scratch testing to a load of 122 mN.

Other studies have also examined the effect of CNT incorporation on the mechanical properties of organic and hybrid coatings. At the low SWCNT loading studied by Fraser et al. in their PMMA–SWCNT composites, no clear benefit was seen in the tensile properties, although there was some evidence to suggest that composites with acid-treated SWCNTs had improved impact strength in comparison with pure PMMA [29].

In their recent study on epoxy–CNT composite coatings deposited on 2024-T3 aluminum alloy substrates, Khun et al. were able to conclude that 0.5 wt.% CNT loading clearly produced composites with improved adhesion to the substrates and improved wear resistance relative to the unloaded epoxy coatings [12]. This improvement was explained in terms of a relaxation of the residual stress within the epoxy coating caused by the incorporation of the CNTs.

Kumar and Gasem have been able to demonstrate the beneficial effects of incorporating 2 wt. % of functionalized MWCNTs into polyaniline (PANI) coatings deposited on mild steel by dip coating [36]. The PANI–MWCNT coatings showed a Vickers micro hardness of 385 HV, compared with 266 HV for pure PANI coatings. Furthermore, PANI–MWCNT coatings showed significantly improved resistance to scratching in comparison with pure PANI coatings.

Despite the results obtained by Fraser et al. [29], the clear trend in the results of the work reported here and elsewhere is that controlled incorporation of CNTs into hybrid and polymer matrices at suitable levels is likely to be beneficial to the matrices in terms of improved mechanical performance. Thus, it is reasonable to expect significant improvements in terms of scratch and wear resistance, adhesion strength and also hardness and Young´s modulus of the matrices when incorporating CNTs. For the most part, this can be attributed to the excellent mechanical properties of the CNTs. However, more work is clearly required to understand fully the mechanism responsible for the beneficial effect of incorporating CNTs on the adhesion of these matrices to metallic substrates.

3.2.5. Anticorrosive properties

The corrosion protection efficiency of the pure and the modified hybrid coatings was determined by EIS, performed in an electrochemical cell containing aqueous 3.5% NaCl solution at 25°C. The principle of EIS is to impose a small sinusoidal potential with varying frequency and, by measuring the alternating current response, to obtain the impedance of the electrochemical system. The impedance $Z(\omega)$ is composed of a real and an imaginary part, involving the ohmic and capacitive contributions, and can be represented as a vector of length $|Z|$, where $|Z| = (Z_{real}^2 + Z_{imag}^2)^{1/2}$. The angle between the Z vector and the Z_{real} axis is the phase angle ϕ [37]. For each measurement, three graphs were obtained: a Nyquist plot (Z_{real} vs. Z_{imag}) and two Bode graphs of the impedance modulus and phase angle as a function of frequency.

EIS measurements were performed for all hybrid-coated samples after one day of immersion and then at 1 week intervals until a significant drop of the impedance modulus occurred due to pitting. The time interval until the onset of pitting defined the lifetime of the coating. The Nyquist and Bode plots are shown in **Figure 16**, while the equivalent electrical circuits of the electrolyte–coating–substrate system used to fit the EIS data are shown in **Figure 17**. For comparison, EIS characteristics of bare A1020 carbon steel substrate were also recorded, as shown in **Figure 16**. The impedance modulus at low frequency and the phase angle behavior is an indicator of the anticorrosion performance. Coatings with modulus higher than 10^8 Ω cm^2 typically provide excellent protection, while those below 10^6 Ω cm^2 have poor protection efficiency [38].

The BPO0.01 matrix had an initial impedance modulus of 10^8 Ω cm^2 which remained unchanged during 56 days it survived testing, while the BPO0.05 matrix had a one order of magnitude higher impedance modulus of 10^9 Ω cm^2, remaining stable for its lifetime of 21 days. This finding might be related to the higher overall connectivity of the BPO0.05 hybrid, which, on the basis of the results of NMR, TG/DTG and mechanical testing, had highly polymerized organic moieties densely interconnected with reticulated silica nodes. This excellent performance of the PMMA–silica hybrid coating can be compared with the performance of the bare carbon steel. The coated samples showed up to 5 orders of magnitude higher corrosion resistance, a consequence of the dense structure acting as an efficient diffusion barrier against aggressive agents. In this context, it should be noted that the anticorrosive performance reported for most hybrid coatings, in terms of initial impedance modules, is usually of the order of 10^7 Ω cm^2 [5, 39, 40].

http://dx.doi.org/10.5772/62808

The addition of CNTs dispersed in SDS in the BPO0.01 matrix did not change neither the impedance modulus (10^8 Ω cm^2) significantly, nor the lifetime of the coating (43 days). The addition of functionalized and dispersed CNTs to the BPO0.05 matrix increased the impedance modulus, but decreased the lifetime of the coating to 7 days for BPO0.05_CNT_SDS and 10 days for BPO0.05_CNTCOOH. As has been suggested in recent studies [12, 13], CNTs act in the PMMA–silica nanocomposite as structural reinforcements and densifier agents, providing improved thermal and mechanical properties without degrading the chemical barrier characteristics. The extraordinary electrochemical performance of these micron thick films, approaching that of thick paints, is related to their dense hybrid structure, thus providing an efficient passivation of metallic surfaces [4]. Although the CNT-containing coatings were thicker than pure hybrid films, they actually showed shorter lifetimes in the NaCl solution. This can be explained in terms of electrolyte uptake via diffusion paths along the outer nanotube walls and also through the cavities of the nanotubes. Therefore, the degradation of the coatings after long-term exposure is associated with the penetration of the electrolyte, involving Cl^- ions, oxygen and water and subsequent chemical reaction (corrosion) at the coating/metal interface [38], causing a sudden drop of the electrochemical performance.

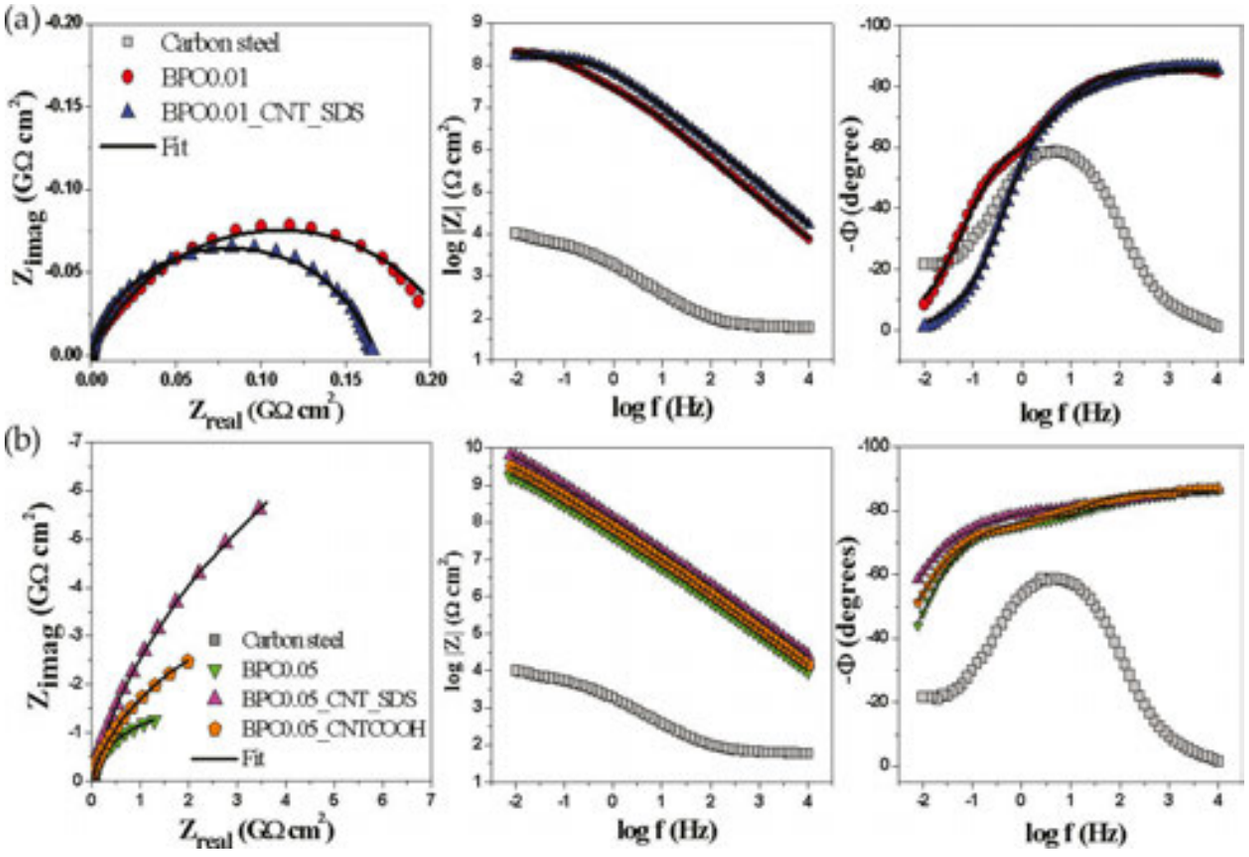

Figure 16. Nyquist and Bode plots for uncoated carbon steel (a) BPO0.01 matrix and (b) BPO0.05 matrix after 1 day of immersion in 3.5% NaCl standard saline solution.

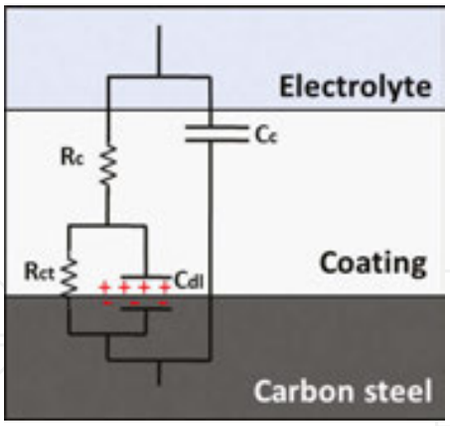

Figure 17. The electrical equivalent circuit used to fit all the EIS experimental data.

To obtain a quantitative model of the electrochemical system, the equivalent circuit of **Figure 17** was used to fit the impedance data of Figure 16. The circuit consists of two time constants, R_c/C_c at high frequency (~10^4 Hz) and R_{ct}/C_{dl} at low frequency (~1 Hz), where R_c is the coating resistance, C_c is the coating capacitance, R_{ct} is the charge transfer resistance and C_{dl} is the capacitance of the electric double layer of the coating/carbon steel interface [38]. As frequently applied for electrochemical systems, the capacitors were replaced by a constant phase element (CPE) to take into account the nonideality of the capacitor representing the coating, expressed by the n_c and n_{dl} exponents. All circuit parameters obtained by fitting the EIS data are shown in **Table 4**. All chi-square (χ^2) values were smaller than 10^{-3}, ensuring a high fit quality. Coatings showing a combination of high corrosion resistance and low phase angle values close to −90°, indicative of ideal capacitive behavior, are very efficient in blocking the electrolyte uptake. All hybrid films showed elevated volume and interface resistances and high-frequency phase angle values below −80° over four decades, all of which are characteristics expected for efficient protective coatings.

	BPO0.01		BPO0.01_CNT_SDS		BPO00.5		BPO005_CNT_SDS		BPO005_CNTCOOH	
χ^2	1.4×10^{-3}		3.0×10^{-4}		3.0×10^{-4}		2.3×10^{-4}		4.4×10^{-4}	
R_C (Ω cm^2)	2.8×10^7	(3.80)	1.3×10^7	(8.77)	1.5×10^7	(5.52)	1.0×10^7	(10.7)	1.5×10^7	(5.52)
CPE_C (Ω^{-1}cm^{-2}s^n)	3.8×10^{-9}	(1.00)	1.5×10^{-9}	(0.96)	2.7×10^{-9}	(0.77)	9.5×10^{-10}	(1.25)	2.7×10^{-9}	(0.77)
n_C	0.95	(0.13)	0.96	(0.10)	0.95	(0.09)	0.96	(0.13)	0.95	(0.09)
R_{ct} (Ω cm^2)	1.9×10^8	(1.32)	1.6×10^8	(1.09)	3.8×10^9	(1.23)	2.6×10^{10}	(1.74)	3.8×10^9	(1.23)
CPE_{dl} (Ω^{-1}cm^{-2}s^n)	7.3×10^{-9}	(1.52)	1.7×10^{-9}	(1.29)	2.2×10^{-9}	(0.91)	6.6×10^{-10}	(1.76)	2.2×10^{-9}	(0.91)
n_{dl}	0.74	(1.27)	0.65	(0.93)	0.70	(0.33)	0.70	(0.43)	0.70	(0.33)

*Values in brackets represent the errors in percentage.

Table 4. Equivalent circuit parameters for all samples after 1 day in 3.5% NaCl solution.

http://dx.doi.org/10.5772/62808

There are a number of related studies which have examined the electrochemical performance of CNT–hybrid and CNT–polymer nanocomposite coatings in contact with saline environments. Liu et al. modified bis-[triethoxysilylpropyl] tetrasulfide (BTESPT) silane films by MWCNTs functionalized with carboxylic groups [41]. EIS results, obtained for coated 304 stainless steel samples in 3.5 % NaCl solution, showed that the addition of different amounts of CNTs (0.5, 2.5 and 5 mg) improved the corrosion resistance relative to the pure BTESPT coatings. The impedance modulus of the BTESPT/MWCNT hybrid film reached about 10^7 Ω cm^2, a value about three orders of magnitude higher than the bare substrate and one order of magnitude higher than the pure BTESPT film. The authors suggested that carboxylated MWCNTs react with silanol groups from the silane precursor to form covalent bonds between BTESPT and the MWCNTs which strengthen the adhesion strength of the film, increasing its density and thus inhibiting the penetration of the corrosive ions. In addition, it was suggested by these authors that the long chain structure of the CNTs may be able to fill pits and cracks in the film, thus helping to reduce the number of corrosion-induced defects.

Jeon et al. reported EIS results combined with hygrothermal cyclic testing of their CNT-loaded epoxy coatings deposited on carbon steel [42]. In the hygrothermal testing, the temperature was ramped up from 25°C to 85°C and back to 25°C over a period of 12 hours while the coating was in contact with the electrolyte. This procedure was designed to accelerate the cumulative effect of the electrolyte on the coating/substrate interface. They found that after 30 hygrothermal test cycles the impedance modulus for pure epoxy coatings at 0.01 Hz decreased from 10^{10} Ω cm^2 to 10^6 Ω cm^2. For the two loadings of 0.25 and 0.5 wt.% that they examined for the CNT-containing samples, there was a lower initial resistance at 0.01 Hz because of the conductive nature of the CNTs, but after 30 cycles the impedance modulus at this frequency was higher than for the pure epoxy coatings. These results were explained by the authors in terms of the decrease in the water uptake of the CNT-loaded coatings, rather than any decrease in chemical attack by the 0.5 wt% NaCl solution, and the increase in adhesion strength of the coatings with the addition of the CNTs.

The anticorrosive performance of epoxy–CNT composite coatings was also reported for aluminum alloy 2024-T3 substrates, tested by EIS in a 0.5 M NaCl solution by Kuhn et al. [12]. Epoxy coatings and epoxy coatings containing 0.1 wt.% of MWCNTs had a impedance modulus of 3×10^4 Ω cm^2, slightly higher than bare Al, which had an impedance modulus of 10^4 Ω cm^2. On comparison, epoxy coatings containing 0.5 wt.% of MWCNTs had a higher impedance modulus of 6×10^4 Ω cm^2, explained by the authors in terms of the 3D dispersion of the MWCNTs in the epoxy matrix at this level contributing to a reduction in the porosity of the coating, and thus reducing its electrolyte uptake.

Deyab [43] studied the effect on the corrosion protection efficiency of coated carbon steel of different CNT concentrations from 0.2 to 0.5 wt.% in alkyd resin films used as the protective coatings. He found that all CNT-loaded films had an improved corrosion resistance in 3.5 wt. % NaCl saline solution relative to the pure alkyd resin films. These findings were attributed to the ability of the functionalized CNTs to absorb resin on their surfaces, thereby enhancing the density of the coatings, eliminating microflaws in the coating and making it more difficult for corrosive species to be transported through the coating to the underlying steel.

Finally, the corrosion protection performance of the PANI–MWCNT coatings studied by Kumar and Gasem demonstrated improved corrosion performance of the coating containing MWCNT in comparison with the pure PANI coatings [36]. This observation was also explained by the authors in terms of a reduced level of porosity in the PANI coating as a consequence of bonding between the PANI matrix and the functionalized CNTs, leading in turn to reduced permeability of coating to corrosive agents.

In comparison with protective coatings based on organic–CNT composites reported to date in the literature, the PMMA–silica–CNT films on carbon steel, discussed in the work, are by far the most effective corrosion protection barrier, with a much higher impedance modulus and lifetime in 3.5% NaCl solution.

Overall, the results obtained in this study have shown that a homogeneous dispersion of single-wall CNTs in PMMA–silica nanocomposites represents a novel and very promising coating system that is able to combine high anticorrosive performance with elevated thermal and mechanical stability, extending the application of these coatings to abrasive environments.

4. Conclusions

Single-wall CNTs have been dispersed through surfactant assistance and by functionalization with carboxylic groups. Both dispersion procedures have proved to be very effective in the modification of PMMA–silica hybrids, producing homogeneous and defect-free nanocomposite coatings with very smooth surfaces (R_{RMS} <0.5 nm) and thicknesses of 2–7 μm. ^{29}Si-NMR results showed that the addition of 500 ppm of CNTs into PMMA–silica hybrid matrices did not affect the high connectivity of the inorganic phase (~80%), while XPS results confirmed the nominal composition and the proportion of bonding environments forming the hybrid network. CNTs were effective in improving the thermal stability of the hybrids, increasing their onset temperature of degradation and shifting all depolymerization events to higher temperatures. Mechanical reinforcement of the hybrid coatings was achieved for both CNT dispersion methods, resulting in a significantly higher scratch resistance and improved adhesion of the coating to A1020 carbon steel substrate relative to the hybrid coatings without the CNTs. EIS results showed that the electrochemical performance of the CNT-loaded coatings is superior to most organic–CNT coating systems reported to date in the literature, being able to act for several weeks as efficient corrosion barriers in aggressive saline environments, maintaining an impedance modulus of up to 10^9 Ω cm^2. These results suggest that CNT-reinforced PMMA–silica nanocomposites have a great potential to extend the applicability of these environmentally compliant, high efficiency anticorrosive coatings to abrasive environments.

Acknowledgements

We would like to thank Dr John Nunn from the National Physical Laboratory, Teddington, U.K. for access to the microscratch equipment used in this work, and the Laboratory for Surface

Science (LCS) at the National Nanotechnology Laboratory (LNNano) in Campinas, Brazil for AFM access. This work was supported by CNPq, CAPES and FAPESP.

Author details

Samarah V. Harb[1], Fábio C. dos Santos[1], Sandra H. Pulcinelli[1], Celso V. Santilli[1], Kevin M. Knowles[2] and Peter Hammer[1*]

*Address all correspondence to: peter@iq.unesp.br

1 Instituto de Química, UNESP-UniversidadeEstadualPaulista, Araraquara, SP, Brazil

2 University of Cambridge, Department of Materials Science and Metallurgy, Cambridge, England

References

[1] Sanchez C., Belleville P., Popall M., Nicole L. Applications of advanced hybrid organic–inorganic nanomaterials: from laboratory to market. Chem Soc Rev. 2011;40(2):696–753. DOI: 10.1039/C0CS00136H.

[2] Molina E.F., Marçal L., Carvalho H.W.P.De, Nassar E.J., Ciuffi K.J. Tri-ureasil gel as a multifunctional organic–inorganic hybrid matrix. Polym Chem. 2013;4(5):1575–1582. DOI: 10.1039/c2py21049e.

[3] Hammer P., Santos F.C.Dos, Cerrutti B.M., Pulcinelli S.H., Santilli C.V. Highly corrosion resistant siloxane-polymethyl methacrylate hybrid coatings. J Sol–gel Sci Technol. 2012;63(2):266–274. DOI: 10.1007/s10971-011-2672-8

[4] Santos F.C.Dos, Harb S.V., Menu M., Turq V., Pulcinelli S.H., Santilli C.V., Hammer P. On the structure of high performance anticorrosive PMMA-siloxane-silica hybrid coatings. RSC Adv. 2015;5(129):106754–106763. DOI: 10.1039/c5ra20885h.

[5] Sarmento V.H.V., Schiavetto M.G., Hammer P., Benedetti A.V., Fugivara C.S., Suegama P.H., Pulcinelli S.H., Santilli C.V. Corrosion protection of stainless steel by polysiloxane hybrid coatings prepared using the sol–gel process. Surf Coat Technol. 2010;204(16–17):2689–2701. DOI: 10.1016/j.surfcoat.2010.02.022.

[6] Sanctis O. De, Gomez L., Pellegri N., Parodi C., Marajofsky A., Duran A. Protective glass coatings on metallic substrates. J Non Cryst Solids. 1990;121(1–3):338–343. DOI: 10.1016/0022-3093(90)90155-F.

[7] Hammer P., Santos F.C.Dos, Cerrutti B.M., Pulcinelli S.H., Santilli C.V. Carbon nanotube-reinforced siloxane-PMMA hybrid coatings with high corrosion resistance. Prog Org Coat. 2013;76(4):601–608. DOI: 10.1016/j.porgcoat.2012.11.015.

[8] Valentino O., Sarno M., Rainone N.G., Nobile M.R., Ciambelli P., Neitzert H.C., Simon G.P. Influence of the polymer structure and nanotube concentration on the conductivity and rheological properties of polyethylene/CNT composites. Phys E. 2008;40(7):2440–2445. DOI: 10.1016/j.physe.2008.02.001.

[9] Chu C.-C, White K.L., Liu P., Zhang X., Sue H.-J. Electrical conductivity and thermal stability of polypropylene containing well-dispersed multi-walled carbon nanotubes disentangled with exfoliated nanoplatelets. Carbon. 2012;50(12):4711–4721. DOI: 10.1016/j.carbon.2012.05.063.

[10] Gojny F.H., Wichmann M.H.G., Köpke U., Fiedler B., Schulte K. Carbon nanotube-reinforced epoxy-composites: enhanced stiffness and fracture toughness at low nanotube content. Compos Sci Technol. 2004;64(15):2363–2371. DOI: 10.1016/j.compscitech.2004.04.002.

[11] Pham G.V., Trinh A.T., To T.X.H., Nguyen T.D., Nguyen T.T., Nguyen X.H. Incorporation of Fe3O4/CNTs nanocomposite in an epoxy coating for corrosion protection of carbon steel. Adv Nat Sci: Nanosci Nanotechnol. 2014;5(3):035016–035022. DOI: 10.1088/2043-6262/5/3/035016.

[12] Khun N.W., Troconis B.C.R., Frankel G.S. Effects of carbon nanotube content on adhesion strength and wear and corrosion resistance of epoxy composite coatings on AA2024-T3. Prog Org Coat. 2014;77(1):72–80. DOI: 10.1016/j.porgcoat.2013.08.003.

[13] Ashassi-Sorkhabi H., Bagheri R., Rezaei-moghadam B. Sonoelectro-chemical synthesis of PPy-MWCNTs-Chitosan nanocomposite coatings: characterization and corrosion behavior. J Mater Eng Perform. 2015;24(1):385–392. DOI: 10.1007/s11665-014-1297-9.

[14] Zeybek B., Aksun E., Üğe A.. Investigation of corrosion protection performance of poly(N-methylpyrrole)-dodecylsulfate/multi-walled carbon nanotubes composite coatings on the stainless steel. Mater Chem Phys 2015;163:11–23. DOI: 10.1016/j.matchemphys.2015.06.022.

[15] Davoodi A., Honarbakhsh S., Farzi G.A. Evaluation of corrosion resistance of polypyrrole/functionalized multi-walled carbon nanotubes composite coatings on 60Cu–40Znbrass alloy. Prog Org Coat 2015;88:106–115. DOI: 10.1016/j.porgcoat.2015.06.018.

[16] Bailey B.M., Leterrier Y., Garcia S.J., Zwaag S.V.D., Michaud V. Electrically conductive self-healing polymer composite coatings. Prog Org Coat 2015;85:189–198. DOI: 10.1016/j.porgcoat.2015.04.013.

[17] Alves da Cunha J.R., Fantini C., Andrade N.F., Alcantara P., Saraiva G.D., Filho A.G.S., Terrones M., Santos M.C.Dos. Enhanced solubilization of carbon nanotubes in aqueous

suspensions of anionic–nonionic surfactant mixtures. J Phys Chem C. 2013;117(47): 25138–25145. DOI: 10.1021/jp4084663.

[18] Brinker C.J., Scherer G.W., editors. Sol–gel science: the physics and chemistry of sol–gel processing. San Diego, CA, Academic Press; 1990. 908 p. DOI: 10.1016/B978-0-08-057103-4.50002-7

[19] Tiwari A., Hihara L.H. Effect of inorganic constituent on nanomechanical and tribological properties of polymer, quasi-ceramic and hybrid coatings. Surf Coat Technol. 2012;206(22):4606–4618. DOI: 10.1016/j.surfcoat.2012.05.020.

[20] Briggs D., Seah M.P., editors. Practical surface analysis: auger and x-ray photoelectron spectroscopy. 2nd ed. Chichester: Wiley; 1990. 674 p.

[21] Naumkin A.V., Kraut-Vass A., Gaarenstroom S.W., Powell C.J. NIST x-ray photoelectron spectroscopy database: NIST standard reference database 20 [Internet]. [Updated: 2012. Available from: http://srdata.nist.gov/XPS/ [accessed: 01/2016].

[22] Sassi Z., Bureau J.C., Bakkali A. Spectroscopic study of TMOS-TMSM-MMA gels: previously identification of the networks inside the hybrid material. Vib Spectrosc. 2002;28(2):299–318. DOI: 10.1016/S0924-2031(02)00009-7.

[23] Wang Y.T., Chang T.C., Hong Y.S., Chen H.B. Effect of the interfacial structure on the thermal stability of poly(methyl methacrylate)-silica hybrids. Thermochim Acta. 2003;397(1–2):219–226. DOI: 10.1016/S0040-6031(02)00327-1.

[24] Kashiwagi T., Inaba A., Brown J.E., Hatada K., Kitayama T., Masuda E. Effects of weak linkages on the thermal and oxidative degradation of poly(methyl methacrylates). Macromolecules. 1986;19(8):2160–2168. DOI: 10.1021/ma00162a010.

[25] Jin Z., Pramoda K.P., Xu G., Goh S.H. Dynamic mechanical behavior of melt-processed multi-walled carbon nanotube/poly(methyl methacrylate) composites. Chem Phys Lett. 2001;337(1–3):43–47. DOI: 10.1016/S0009-2614(01)00186-5.

[26] Troitskii B.B., Troitskaya L.S., Yakhnov A.S., Lopatin M.O., Novikova M.A. Retardation of thermal degradation of PMMA and PVC by C60. Eur Polym J. 1997;33(10–12):1587–1590. DOI: 10.1016/S0014-3057(97)00048-7.

[27] Sabet S.M., Mahfuz H., Terentis A.C., Hashemi J., Boesl B. A facile approach to the synthesis of multi-walled carbon nanotube-polyhedral oligomeric silsesquioxane (POSS) nanohybrids. Mater Lett 2016;168:9–12. DOI: 10.1016/j.matlet.2015.12.149.

[28] Zhang T., Du Z., Zou W., Li H., Zhang C. The flame retardancy of blob-like multi-walled carbon nanotubes/silica nanospheres hybrids in poly (methyl methacrylate). Polym Degrad Stab. 2012;97(9):1716–1723. DOI: 10.1016/j.polymdegradstab.2012.06.014.

[29] Fraser R.A., Stoeffler K., Ashrafi B., Zhang Y., Simard B. Large-scale production of PMMA/SWCNT composites based on SWCNT modified with PMMA. ACS Appl Mater Interfaces. 2012;4(4):1990–1997. DOI: 10.1021/am201824k.

[30] Xiong J., Zheng Z., Qin X., Li M., Li H., Wang X. The thermal and mechanical properties of a polyurethane/multi-walled carbon nanotube composite. Carbon. 2006;44(13):2701–2707. DOI: 10.1016/j.carbon.2006.04.005.

[31] Wei H., Ding D., Wei S., Guo Z. Anticorrosive conductive polyurethane multiwalled carbon nanotube nanocomposites. J Mater Chem A. 2013;1(36):10805–10813. DOI: 10.1039/C3TA11966A.

[32] Mammeri F., Bourhis E.Le, Rozes L., Sanchez C. Elaboration and mechanical characterization of nanocomposites thin films: Part I: Determination of the mechanical properties of thin films prepared by in situ polymerisation of tetraethoxysilane in poly(methyl methacrylate). J Eur Ceram Soc. 2006;26(3):259–266. DOI: 10.1016/j.jeurceramsoc.2004.11.013.

[33] Callister W.D., Rethwisch D.G. Appendix B/Properties of Selected Engineering Materials. In: Callister W.D., Rethwisch D.G., editors. Fundamentals of materials science and engineering: an integrated approach. 4th ed. Hoboken: Wiley; 2012. pp. 835–836.

[34] Harb S.V., Cerrutti B.M., Pulcinelli S.H., Santilli C.V., Hammer P. Siloxane-PMMA hybrid anti-corrosion coatings reinforced by lignin. Surf Coat Technol 2015;275:9–16. DOI: 10.1016/j.surfcoat.2015.05.002.

[35] Eder D. Carbon nanotube-inorganic hybrids. Chem Rev. 2010;110(3):1348–1385. DOI: 10.1021/cr800433k.

[36] Kumar A.M., Gasem Z.M. Effect of functionalization of carbon nanotubes on mechanical and electrochemical behavior of polyaniline nanocomposite coatings. Surf Coat Technol 2015;276:416–423. DOI: 10.1016/j.surfcoat.2015.06.036.

[37] Macdonald J.R., Johnson W.B. Fundamentals of impedance spectroscopy. In: Barsoukov E., Macdonald J.R., editors. Impedance Spectroscopy: Theory, Experiment, and Applications. 2nd ed. Hoboken, NJ, USA: John Wiley & Sons; 2005. 1–26. DOI: 10.1002/0471716243.ch1.

[38] McIntyre J.M., Pham H.Q. Electrochemical impedance spectroscopy; a tool for organic coatings optimizations. Prog Org Coat. 1996;27(1–4):201–207. DOI: 10.1016/0300-9440(95)00532-3.

[39] Sakai R.T., Di F.M., Cruz L.Da, Melo H.G.De, Benedetti A.V., Santilli C.V., Suegama P.H. Electrochemical study of TEOS, TEOS/MPTS, MPTS/MMA and TEOS/MPTS/MMA films on tin coated steel in 3.5% NaCl solution. Prog Org Coat. 2012;74(2):288–301. DOI: 10.1016/j.porgcoat.2012.01.001.

[40] Asadi N., Naderi R., Saremi M., Arman S.Y., Fedel M., Deflorian F. Study of corrosion protection of mild steel by eco-friendly silane sol–gel coating. J Sol–gel Sci Technol. 2014;70(3):329–338. DOI: 10.1007/s10971-014-3286-8.

[41] Liu Y., Cao H., Yu Y., Chen S. Corrosion protection of silane coatings modified by carbon nanotubes on stainless steel. Int J Electrochem Sci 2015;10:3497–3509.

[42] Jeon H., Park J., Shon M. Corrosion protection by epoxy coating containing multi-walled carbon nanotubes. J Ind Eng Chem. 2013;19(3):849–853. DOI: 10.1016/j.jiec.2012.10.030.

[43] Deyab M.A. Effect of carbon nano-tubes on the corrosion resistance of alkyd coating immersed in sodium chloride solution. Prog Org Coat 2015;85:146–150. DOI: 10.1016/j.porgcoat.2015.04.003.

IntechOpen